Applied Catalysis B: Environmental 138–139 (2013) 260–267

Contents lists available at SciVerse ScienceDirect

Applied Catalysis B: Environmental

journal homepage: www.elsevier.com/locate/apcatb

Selective synthesis of TiO_2-based nanoparticles with highly active surface sites for gas-phase photocatalytic oxidation

Yijiao Jiang, Rose Amal*

ARC Centre of Excellence for Functional Nanomaterials, School of Chemical Engineering, The University of New South Wales, Sydney, NSW 2052, Australia

ARTICLE INFO

Article history:
Received 28 August 2012
Received in revised form 7 February 2013
Accepted 10 February 2013
Available online 26 February 2013

Keywords:
Photocatalytic oxidation
Titanium dioxide
Surface hydroxyl groups
^{1}H MAS NMR
Acetaldehyde
Ethanol

ABSTRACT

This work demonstrated the absence of surface terminal hydroxyl groups plays a key role in the photocatalytic oxidation of low concentration volatile organic compounds. Probed by ^{1}H MAS NMR spectroscopy, we showed the synthesis of bare and F-TiO_2 nanoparticles with undetectably low content of terminal hydroxyl groups (TiOH) on the surface of TiO_2 could be obtained through a sol–gel process. The characterization results by N_2 adsorption, XRD, HRTEM, Raman, and XPS show that the bare TiO_2 and F-TiO_2 have almost identical bulk and surface structural properties. The photocatalytic activity was evaluated by photocatalytic oxidation of acetaldehyde and ethanol. Due to the absence of terminal TiOH in the bare TiO_2 and F-TiO_2, both materials exhibit 100% photodegradation of acetaldehyde and ethanol. No deactivation was observed during the experimental period of 8 days. The activities surpassed the photodegradation performance of the benchmarking Aeroxide P25 TiO_2 under similar conditions (93%). On the bare TiO_2, only stoichiometric CO_2 production was observed and no detectable by-product existed in the product stream, resulting in no expanded off-odor problems. On the contrary, ethanol photodegradation on F-TiO_2 produced minor acetaldehyde as a by-product, but the amount of acetaldehyde produced was still lower than that produced on Aeroxide P25.

1. Introduction

Indoor environments such as aircraft cabin, office building, and road vehicles typically contain higher level of volatile organic compounds (VOCs) than outdoors. Exposure to these pollutants can cause headache, nausea, fatigue and other symptoms referred as sick building syndrome. Recently, heterogeneous photocatalysis has gained wide popularity, owing to its widespread applications in environmental remediation and clean energy production [1,2]. Of particular interest is the photocatalytic oxidation (PCO) of low concentration volatile organic compounds. Since the discovery of photocatalytic properties of titanium dioxide (TiO_2) by Fujishima and Honda [3], TiO_2 has been considered as the most efficient and environmentally benign photocatalysts, in which the photogenerated electrons and holes migrate to the nanocrystal surface as redox sites, ultimately leading to the destruction of VOCs [4]. Potential applications of TiO_2 would be more wide spread if highly active TiO_2 can be synthesized to overcome problems of catalyst deactivation and harmful by-product generation under continuous-flow conditions.

To this end, one of the most intensive research areas is to look for the crucial relationships between the structural properties and the photocatalytic activities. It has been well established that the photocatalytic activity of TiO_2 is strongly dependent on the light absorption properties, reduction and oxidation rates on the surface by the electron and hole, and the electron-hole recombination rate [2]. It has been reported that larger specific surface area (SSA), high crystallinity, mixed crystal phases, more preferentially-exposed crystallographic facets, and less defective bulks, generally contribute to higher photocatalytic activities [4]. Very recently, our work has revealed that the photocatalytic activity of the TiO_2 synthesized by one-step flame spray pyrolysis (FSP) method is directly related to the presence of surface terminal hydroxyl groups present on TiO_2, which can be sensitively detected by high-field ^{1}H MAS NMR [5]. It was found that TiO_2 with a low content of surface terminal hydroxyl groups showed a high photocatalytic activity in oxidizing gaseous acetaldehyde (ACE). To design a better TiO_2 photocatalyst with the disappearance of surface terminal TiOH, it is crucial to control their formation pathways. The terminal TiOH mostly reside at defective sites. Ideally, TiO_2 should be highly crystalline to avoid the formation of detrimental defective sites. The synthesis of TiO_2 nanoparticles from hydrolysis of titanium alkoxide precursors via a sol–gel route has been studied extensively [4,6]. Different particle sizes and shapes of TiO_2 could be obtained by adjusting the synthesis parameters. Polymeric Ti—O—Ti chains

* Corresponding author. Tel.: +61 2 9385 4361; fax: +61 2 9385 5966.
E-mail address: r.amal@unsw.edu.au (R. Amal).

0926-3373/$ – see front matter © 2013 Elsevier B.V. All rights reserved.
http://dx.doi.org/10.1016/j.apcatb.2013.02.026

could be developed in the presence of a large excess of water in case of using titanium tetraisopropoxide (TTIP) as a Ti precursor, whereas the formation of $Ti(OH)_4$ is favored with high hydrolysis rates with a medium water amount [7]. From the study on the growth kinetics of TiO_2 nanoparticles in aqueous solution, secondary particles are formed by epitaxial self-assembly of primary particles at longer times and higher temperatures.

In this work, pre-designed bare and fluorinated TiO_2 (F-TiO_2) nanoparticles, both with extremely low contents of terminal hydroxyl groups present on the surface, have been synthesized. After fully characterized the particles by ^{1}H MAS NMR, N_2 adsorption, HRTEM, Raman and XPS spectroscopies, the photocatalytic activity of both materials to oxidize ACE and ethanol, as representative gaseous pollutants in indoor environments, were also studied.

2. Experimental

2.1. Catalyst preparation

Titanium tetraisopropoxide (TTIP, Aldrich, 97%) and hexafluorobenzene (HFB, Aldrich, 99%) used as a titanium and fluorine precursor, respectively, were used as received without further purification. Bare TiO_2 and F-TiO_2 nanoparticles were prepared by a simple sol–gel method described as follows: 10 ml of TTIP as received was added dropwise to 250 ml Milli-Q water under mechanical stirring at room temperature. No precipitate could be recovered. The solution was sonicated for 30 min without cooling, so that a temperature of ca. 323 K was reached. Subsequently, the solution was aged in a closed beaker at room temperature for 2 days, and then dried at 373 K until complete evaporation of residual water (ca. 30 h). The dried powders were calcined at 773 K for 1 h to enhance crystallization of TiO_2. The temperature ramp rate was approximately 10 K/min and cooled down naturally. To synthesize F-TiO_2, 2 ml of hexafluorobenzene was added into the 10 ml TTIP to obtain a nominal Ti/F atomic ratio of 2, followed by the same procedure to synthesize the bare TiO_2.

2.2. Surface hydroxyl groups determined by ^{1}H MAS NMR

High-field ^{1}H MAS NMR experiments were performed on a Bruker Avance III 700 spectrometer at a resonance frequency of 700.36 MHz for ^{1}H nuclei. Single-pulse excitation corresponding to a $\pi/2$ flip angle with repetition time of 1 s was used. An ultrahigh-speed 2.5 mm Bruker MAS probe at a sample spinning rate of 25 kHz was used. Typically, 128 transients were acquired using a small pulse angle (2.1 μs pulse width). The chemical shifts were measured relative to 4,4-dimethyl-4-silapentane-1-sulfonic acid (DSS) as an external standard. The solid-state NMR spectra were processed using the Bruker software TOPSPIN 3.0. The samples were directly analyzed after calcination without any further treatment.

2.3. Catalyst characterization

X-ray diffraction (XRD) patterns were recorded on a Philips X'pert multipurpose X-ray diffraction system using Cu $K\alpha_1$ (λ = 1.5406 Å) radiation at 45 kV and 40 mA. The Brunauer–Emmett–Teller (BET) specific surface areas were obtained from nitrogen physisorption isotherms (adsorption–desorption branches) at 77 K on a Micromeritics Tristar 3000 instrument. High-resolution transmission electron microscopy (HRTEM) investigations were performed on a Philips CM200 microscope (FEI; LaB_6 cathode, operated at 200 kV, point resolution ~2 Å). Raman spectroscopic studies were carried out (Renishaw InVia Raman) with a 514-nm diode (Argon ion laser) laser as excitation source focused with a microscope (Leica, magnification 50×). The spectra were collected on a CCD camera after being diffracted by 1800 lines per millimeter grating using 24.7-mW laser energy. X-ray photoelectron spectra (XPS) were collected on an ESCALAB250Xi spectrometer employing a mono-chromated Al Kα (1486.68 eV) X-ray source operated at 15.2 kV and 168 W. The photoelectron take-off angle was 90° measured with respect to the surface of the sample. Survey (wide-scan) spectra were obtained with pass energy of 100 eV. Surface narrow-scan spectra with pass energy of 20 eV were obtained for the C 1s, O 1s, Ti 2p, and F 1s photopeaks. All binding energies were referenced to the carbon C—H photopeak at 285.0 eV.

2.4. Photocatalytic activity test

Photocatalytic oxidation of gaseous ACE or ethanol on TiO_2 photocatalyts was carried out in a continuous-flow packed bed annular glass photoreactor described elsewhere [8]. Briefly, the annular reactor consisted of a closed 11.1 mm diameter glass tube inserted into an open ended glass tube (11.3 mm ID, 15.0 mm OD), which gave an average annular spacing of 0.1 mm width. The four lamps (NEC FL6BL-B UV-A lamps, 6 W, λ_{max} = 355 nm) were symmetrically positioned around the photoreactor with separation distance of 5 cm. This setup was housed within a UV black box and fitted with a fan to ensure the constant temperature. Typically, 20 mg of photocatalyst was diluted with 240 mg of silica beads (100 μm diameter) and kept in place between two quartz wool plugs. Prior to photocatalytic oxidation, the target gas diluted with dry air (initial ACE concentration = 183 ± 10 ppm and ethanol concentration = 178 ± 10 ppm) was pre-adsorbed on the catalyst without illumination until saturation was achieved. Subsequently, the oxidation was commenced with the four lamps turned on. The effluent stream continued to be sampled periodically (10 min) and analyzed using an on-line gas chromatograph (Shimadzu 2010, HP-PLOT/Q capillary column) with a flame ionization detector (FID) and methanizer. A blank run (photoreactor filled with only quartz wool and silica beads) showed no conversion at the reaction conditions used.

3. Results and discussion

3.1. Catalyst preparation

It is well established that the formation of the Ti—O—Ti network proceeds via a hydrolysis step followed by polycondensation [9]. In most sol–gel methods, massive precipitation of amorphous TiO_2 is generally accompanied by uncontrolled branching of the resulting Ti—O—Ti network, since hydrolysis is very fast and nucleation and growth was completed within seconds [7]. Many efforts have been exerted to achieve highly crystallized TiO_2 nanoparticles by controlling hydrolysis conditions. In this context, ultrasound irradiation can be employed to break up the aggregates into very small aggregates and primary particles, which are most likely defect-free and less terminal TiOH on the surface of TiO_2. Assisted by ultrasound irradiation, many localized hot spots within the homogeneous gel are generated and result in the acceleration of polycondensation of ≡Ti—OH groups. Gedanken and his co-workers demonstrated that anatase was favorably formed when TTIP was used as the Ti precursor in the synthesis of TiO_2 under ultrasound irradiation [10]. Yu et al. have synthesized TiO_2 nanoparticles in pure water or ethanol/water medium under ultrasonic irradiation [11,12]. The hydrolysis temperature and the acidity of the medium had strong influence on the crystallization. It was also found that the slow hydrolysis of TTIP in pure water lead to a nearly neutral and more homogeneous gel.

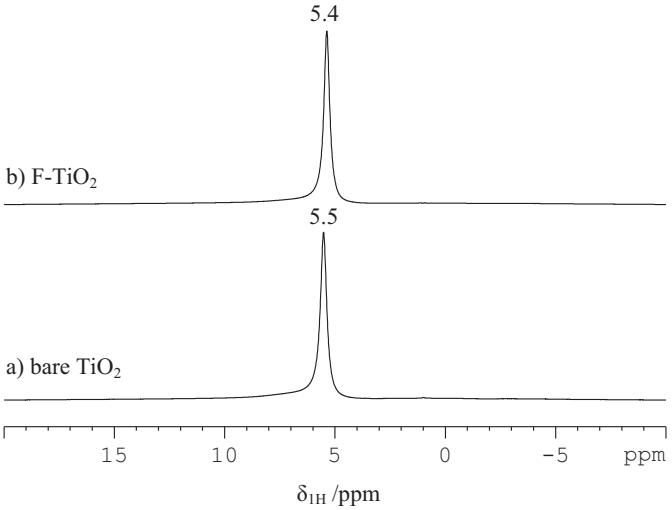

Fig. 1. ^{1}H MAS NMR spectra of bare TiO_2 (a) and F-TiO_2 (b).

In this study, we were attempting to synthesize highly crystallized TiO_2 nanoparticles with less content of terminal TiOH. This was achieved by a simple sol–gel synthetic approach, which relied on dropwise addition of TTIP into a large amount of water to ensure complete hydrolysis of TTIP. The polycondensation was then promoted using ultrasound irradiation, which provided a homogeneous local environment and prevented agglomeration. A prolonged heating time of 30 h at 373 K for the as-prepared gel was used to avoid the agglomeration of the TiO_2 nanoparticles during the crystallization process. Milli-Q water was used as the neutral hydrolysis medium, which would accelerate neither deprotonation nor dehydroxylation during polycondensation. As our previous studies found that the presence of fluorine atoms in the FSP-made TiO_2 could contribute to the decrease of the relative content of terminal TiOH on the surface [5], hexafluorobenzene was employed as fluorine precursor for the sol–gel synthesis of F-TiO_2 in this work.

3.2. Surface hydroxyl groups determined by ^{1}H MAS NMR spectra

Firstly, to verify if we have successfully synthesized the bare TiO_2 and F-TiO_2 with vanishing terminal TiOH groups on the surface, high-field ^{1}H MAS NMR spectroscopy was applied to study the distribution of surface hydroxyl groups present on both TiO_2 samples. The ^{1}H MAS NMR spectra are shown in Fig. 1. As expected, the spectrum of the F-TiO_2 (Fig. 1b) exhibits a sole signal at 5.4 ppm, which is ascribed to the bridging hydroxyl groups (bridging TiOH) [13]. By naked eye, there is no terminal TiOH group at around 1.8 ppm present on the surface of F-TiO_2. The similarity of the spectrum is consistent with our F-modified TiO_2 prepared by flame spray pyrolysis. It implies that the sol–gel method can selectively synthesize F-TiO_2 with undetectable low terminal TiOH groups.

Notably, the high-field ^{1}H MAS NMR spectroscopy did not observe the presence of terminal TiOH groups in the bare TiO_2 as well (see Fig. 1a). Only one peak at 5.5 ppm assigned to bridging TiOH groups was observed. This signal slightly shifted to lower field, which might be due to the changes of electronic properties. The bare TiO_2 is expected to possess a slightly higher acidity in comparison with the above F-TiO_2 (Fig. 1b), as the ^{1}H chemical shift is a sensitive measure for the acid strength of surface OH groups [14]. Obviously, the present bare TiO_2 exhibited a complete disappearance of the signal at ~1.8 ppm assigned to terminal TiOH groups attached to surface impurities. This fact implies that the termination of terminal TiOH groups is possible even without fluorination process using the current synthesis method, which brings

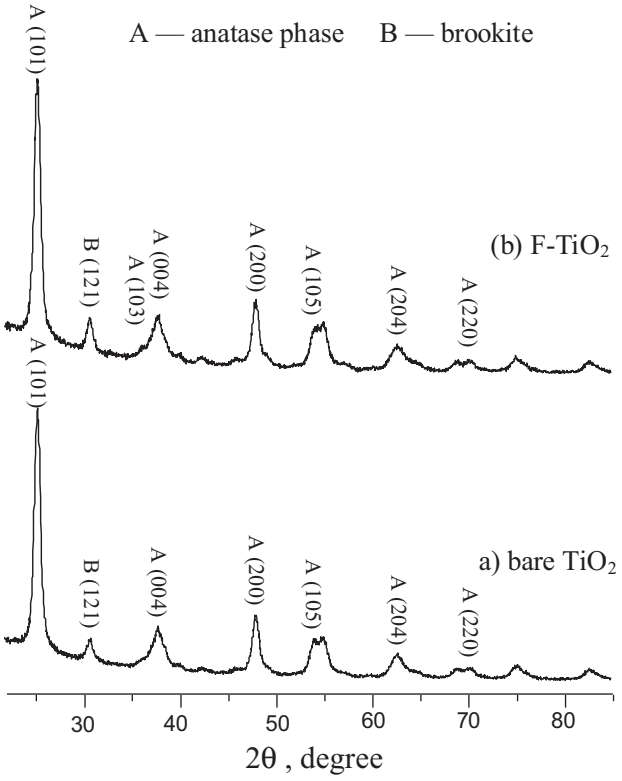

Fig. 2. Powder XRD patterns of bare TiO_2 (a) and F-TiO_2 (b).

our aim to selectively synthesize TiO_2 with less terminal TiOH groups into a reality. As shown in Fig. S1 (see the Supplementary Information), besides the main signal at 5.2 ppm due to the bridging hydroxyl groups, the ^{1}H MAS NMR spectrum for Aeroxide P25 TiO_2 shows two additional weak signals at ca. 1.8 and 0.9 ppm, which is assigned to terminal hydroxyl groups in the anatase and rutile phase, respectively. The signal intensity ratio of bridging and terminal TiOH groups is about 23:1. The terminal hydroxyl groups cannot be detected in the bare TiO_2 and F-TiO_2 present in this study. Prior to testing the photocatalytic activity, both of the bare TiO_2 and F-TiO_2 materials were thoroughly characterized by a wide range of methods, including XRD, N_2 adsorption, HRTEM, Raman, and XPS, to ensure that they have similar features.

3.3. Textural and morphological properties

Fig. 2 shows the XRD patterns of the bare TiO_2 and F-TiO_2. The coexistence of anatase and brookite was observed in the XRD patterns for both samples. The dominant peak at $2\theta = 25^\circ$ is attributed to the anatase (1 0 1) peak (JCPDS No. 21-1272), which is probably overlapped with brookite (1 2 0) and (1 1 1) peaks. A small fraction of the brookite (1 2 1) peak appeared at $2\theta = 31^\circ$ (JCPDS No. 29-1360). No reflection of rutile (1 1 0) peak at 27.5° was observed in both samples. Gedanken found that the pure anatase was formed when TTIP was employed as the precursor, and rutile was obtained when the titanium tetrachloride (TTC) was the precursor, while a mixture of anatase and rutile was obtained when the precursor was a mixture of TTIP and TTC [10]. Our results imply that the preparative conditions can also affect the final crystalline phase of the product. Many studies have confirmed that a mixed phase of anatase/rutile or anatase/brookite with a majority of anatase of TiO_2 exhibits superior photocatalytic activity in degrading organic pollutants [15–17]. The reflections of both samples seem to be quite coincident in terms of both peak intensity and line width. It implies that fluorination does not change the bulk crystal structure of TiO_2.

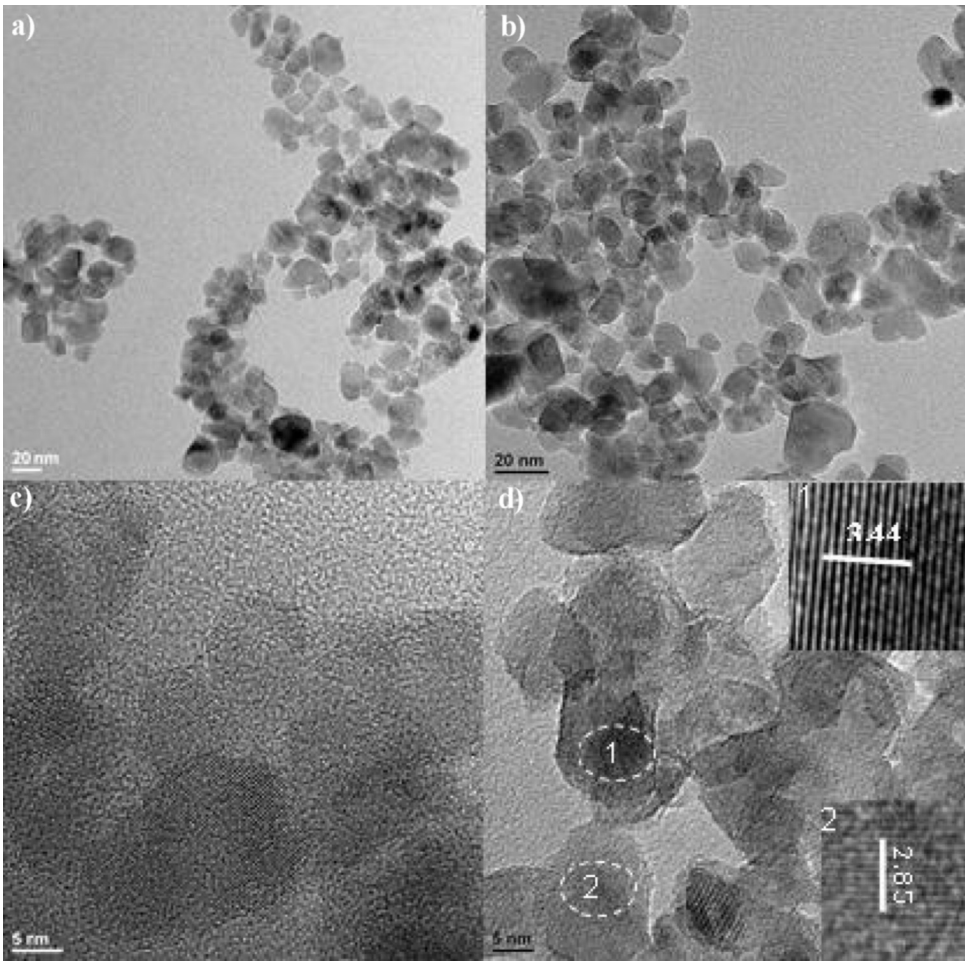

Fig. 3. TEM images of bare TiO_2 (a) and F-TiO_2 (b), and high magnification TEM pictures of bare TiO2 (c) and F-TiO2 (d).

Evaluated by software High Score plus with ICDD database, a ratio of around 4:1 between anatase and brookite phases was determined from crystallite phase analysis.

The bare TiO_2 and F-TiO_2, results in nano-sized catalyst particles with BET specific surface areas (SSA) of 66 and 68 m^2/g, respectively, determined by N_2 adsorption. These surface areas are very close to that of Aeroxide TiO_2 (50 m^2/g). Nitrogen adsorption-desorption isotherms by the Barrett–Joyner–Halenda method provide average pore diameter of 10.0 and 10.3 nm for the bare TiO_2 and F-TiO_2, respectively. Data from N_2 adsorption implies that fluorination of TiO_2 did not virtually influence the pore size distribution as well.

Fig. 3 shows TEM images of the bare TiO_2 and F-TiO_2 nanoparticles. The pictures in Fig. 3a and b show that the samples consist of nearly round particles, having narrow size distributions of the different crystals. The pictures exhibit similar structural and morphological features regardless of the presence of fluorine. The large particles of ~20 nm are assigned to brookite phase, in the thermodynamically stable region; whereas the small particles of ~10 nm attributed to anatase phase are also in the stable region according to the reported finding about size-dependent phase stability [18]. The interference patterns illustrate that the particles are crystalline. High magnification picture of a single nanoparticle shows the growth orientation by identification of the crystal lattice planes. Lattice fringe spacings for nanoparticles in Fig. 3d are 0.34 and 0.29 nm respectively, close to the anatase (1 0 1) *d*-value of 0.35 nm and the brookite (1 2 1) *d*-value of 0.29 nm, respectively [19]. Thus, it is further confirmed that both of the nanoparticles in Fig. 3 consist of anatase and brookite phase, in good agreement with the above XRD results. In summary, the XRD, N_2 adsorption, and TEM measurements reveal that both the samples are composed of identical nanocrystalline TiO_2.

3.4. Raman spectroscopy

Visible Raman spectroscopy is known to be sensitive to the absolute phase composition in the bulk region of TiO_2 because the TiO_2 sample is transparent in the visible region. The phase composition of TiO_2 can be sensitively identified. The high resolution of the bare TiO_2 and F-TiO_2 Raman spectra is a reflection of their high crystallinity. In Fig. 4a, the anatase phase shows major Raman bands at 143, 193, 395, 515, 636 cm^{-1}. The expected band assumed at 519 cm^{-1} may be superimposed with the 515 cm^{-1} band. In good agreement with reported literature, these bands can be attributed to the six Raman-active modes of anatase phase with the symmetries of E_g, E_g, B_{1g}, A_{1g}, B_{1g}, and E_g, respectively [20]. Apparently, the band at 143 cm^{-1} is the strongest one for the anatase phase. The weak Raman bands due to brookite phase occur at 245, 323, 365 cm^{-1}, which can be ascribed to the A_g, B_{1g}, and B_{2g} of characteristic brookite phase, respectively. As a confirmation of XRD analysis, the Raman spectra for both of the TiO_2 samples clearly show that they contain both anatase and brookite. However, the Ti-F vibrations was not detected, which is possibly due to the unstable TiO_xF_y species at ambient conditions and at low concentrations [21]. Compared to the spectra in Fig. 4a, it can be seen that fluorination does not change the position of the Raman bands, their line widths and relative intensities as shown in Fig. 4b. Therefore, it is confirmed that the fluorination does not destroy the microstructures of TiO_2.

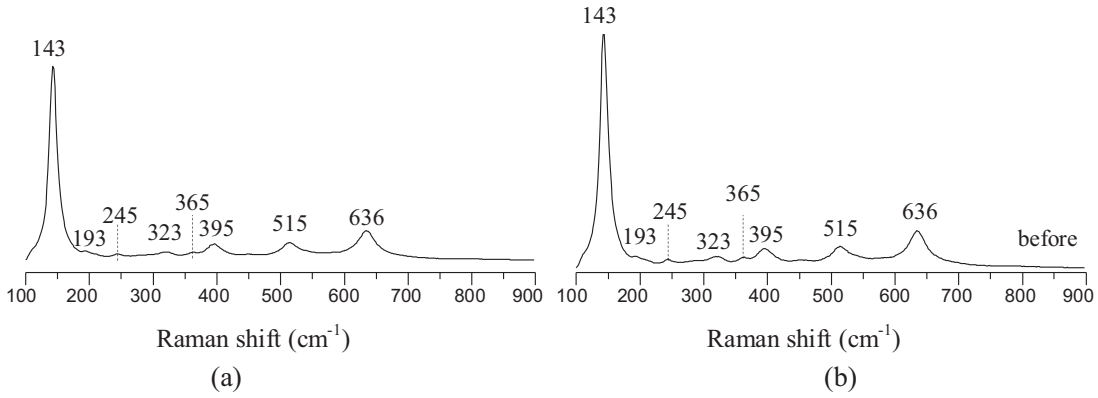

Fig. 4. Raman spectra of bare TiO_2 (a) and F-TiO_2 (b).

3.5. XPS spectra

XPS is a sensitive method to study the surface state of a material, which is often used to determine the oxidation state and element contents on the surface. Fig. 5 shows typical XPS survey (wide-scan) spectra of the bare TiO_2 and F-TiO_2. Obviously, Ti, O, and C elements with comparable peak intensities were present at the surfaces of both the bare and F-TiO_2 samples. The photoelectron peaks of Ti 2p, O 1s, and C 1s appears clearly at bind energies of 457, 530, and 285 eV, respectively [22]. The Ti 2p XPS spectra (not shown) are almost identical for both the bare and F-TiO_2, which indicates that Ti atoms have a similar bonding environment after fluorination. In good agreement with previous report [22], the C 1s peak was resolved into three individual peaks at 285.0 eV for C—H (C—C), 287 eV for C—O, and 289 eV for O—C=O, respectively (not shown).

However, the fluorine content was too low to be detected by two scans on the surface of F-TiO_2 sample. A weak band at around 684 eV in the F-TiO_2 sample was detected after 30 scans (see the insert of Fig. 5b). The surface F 1s state of the F-TiO_2 was defined by a binding energy of 684 eV, which is corresponding to the fluorine ions adsorbed on the TiO_2 surface. The present XPS result of F 1s indicates that the amount fluorine atoms in the F-TiO_2 became very low (ca. 0.3%) upon calcination at 773 K.

3.6. Photocatalytic oxidation of acetaldehyde

In this study, commercial Aeroxide P25 TiO_2 was used as the benchmark photocatalyst for comparison. The photocatalytic activity of the bare TiO2 and F-TiO2 was tested under continuous-flow conditions with a constant gas hourly space velocity (GHSV, 135 L g_{cat}^{-1} h^{-1}). The acetaldehyde (ACE) concentration fed into the reactor was kept constant using adjustments of feed initial ACE (183 ± 10 ppm). As the control experiments, the photodegradation of ACE was not evident when illuminated without photocatalyst or passed through the catalyst bed but without UV illumination. In Fig. 6a, the ACE concentration in the effluent was plotted as a function of dark adsorption time. Approximately, 40 min after the injection of ACE gas into the reactor packed with the bare TiO_2 (filled circles), the adsorption breakpoint was observed. Whereas it took around 60 min until the adsorption breakpoint appeared on the F-TiO_2 (filled cubes). In addition, it appears that the adsorption isotherm slope of the bare TiO_2 was larger than that of F-TiO_2. It indicates that the bare TiO_2 showed faster adsorption rate, while fluorination resulted in a slow-down equilibrium course from the ACE adsorption profile. It implies that the number of adsorption sites is thought to be more on the F-TiO_2. As reported previously, surface fluorination of TiO_2 has been demonstrated to enhance photocatalytic activity for gas-phase reactions in many instances [21,23]. It was proposed that surface fluorination of TiO_2 is an exchange between fluorine ions and surface hydroxyl groups. In this work, no terminal hydroxyl group was accessible for the exchange with the fluorine atoms.

Fig. 6b provides the ACE concentration in the effluent following passage through the bare and F-TiO_2 catalysts bed with UV illumination. These two photocatalysts behaved similarly in many aspects, despite the presence of fluorine in the F-TiO_2 (solid cubes). An exponential decrease of ACE concentration in the effluent was observed just after the UV irradiation on both of the TiO_2 catalysts as shown in Fig. 6b. Both of these two TiO_2 materials exhibit excellent photocatalytic activity (100% conversion), and exceed

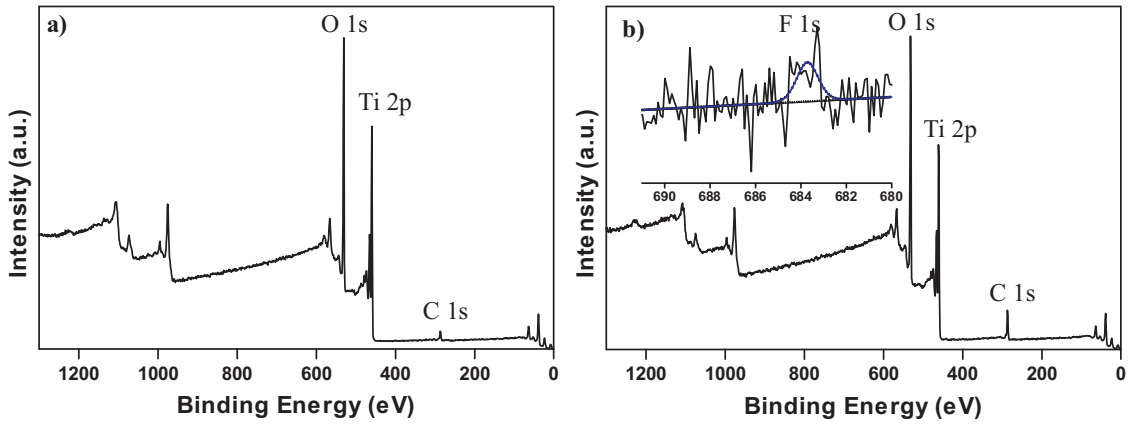

Fig. 5. XPS survey spectra of bare TiO_2 (a) and F-TiO_2 (b). The inset shows the narrow-band XPS of the element F in the F-TiO_2.

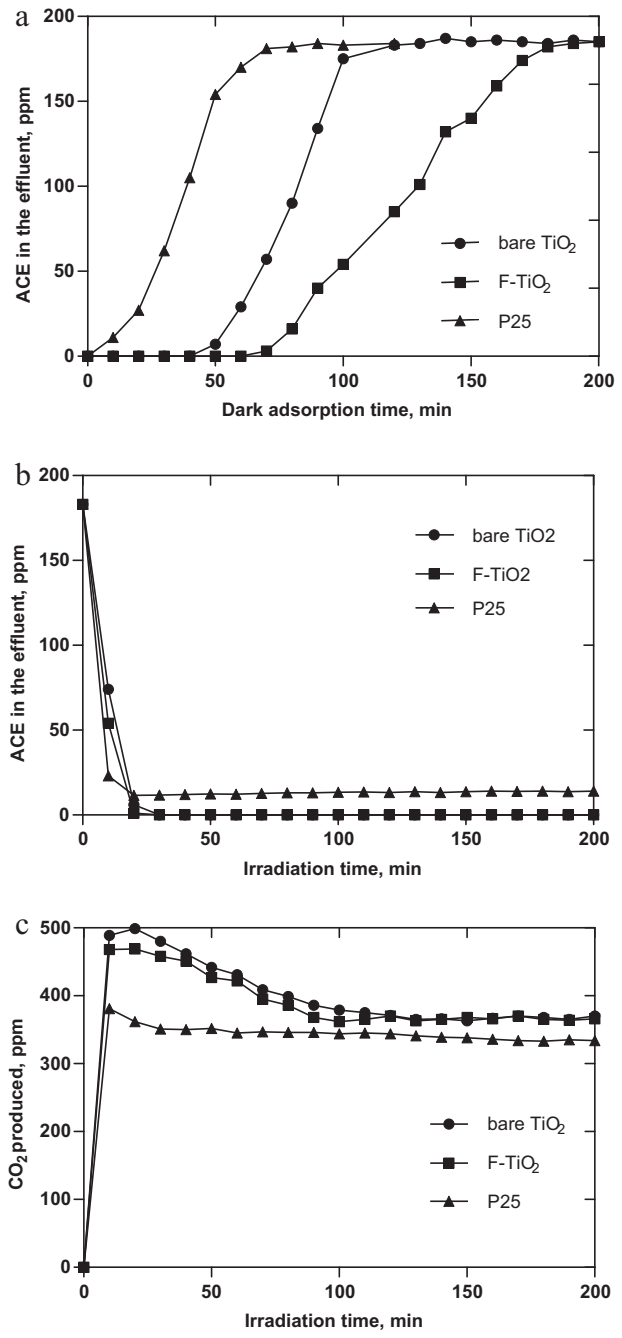

Fig. 6. Dark adsorption profile (a), photodegradation profiles (b), and the corresponding CO_2 produced from photocatalytic oxidation of ACE on bare TiO_2 (●), F-TiO_2 (■), and P25 (▲). Initial ACE concentration = 183 ± 10 ppm.

that of the benchmarking Aeroxide P25 TiO_2, which processed a photodegradation rate of 93% under identical operation conditions (filled triangles).

In addition, the CO_2 produced from ACE photodegradation processes on both of the TiO_2 are also very similar as shown in Fig. 6c; the deviations do not exceed the estimated error of the analysis (±0.5%). This is an indication that the effect of the presence of fluorine in TiO_2 is minor and the bare TiO_2 exhibits excellent photoactivity in ACE photodegradation. It is noted that only in the initial transient period of the photodegradation, a relative small amount of acetic acid as a sole by-product was detected. It indicates that the number of ACE molecules in the initial stage was larger than the number of photons, and as a consequence ACE could be partially oxidized to acetic acid. Under the steady state, ACE was completely oxidized to CO_2. It implies that the number of holes produced in both TiO_2 photocatalysts was much larger than the number of ACE molecules adsorbed on the surface. A stationary CO_2 concentration of ca. 370 ppm was observed. The carbon mass balance under the steady state calculated from CO_2 concentrations was closed within 10%. This closure is within the errors of chromatographic analysis and testifies to the absence of significant gaseous by-products.

3.7. Photocatalytic oxidation of ethanol

The photocatalytic activity of the bare TiO_2 and F-TiO_2 was further assessed by photocatalytic oxidation of gaseous ethanol under identical conditions except for the feeding concentration of ethanol (178 ± 10 ppm). Since the vapour pressure of ethanol (7.88 kPa) is much lower than that of ACE (120 kPa) at room temperature, ACE is expected as the main toxic intermediate during the photocatalytic oxidation of ethanol, resulting in expanded off-odor problems. A plot of ethanol concentration in the effluent as a function of dark adsorption time is shown in Fig. 7a. Obviously, bare TiO_2 shows better adsorption performance than F-TiO_2, presumably because of electrostatic attraction resulting in stronger ethanol adsorption. In the adsorption course on both of the TiO_2 materials, a minor ACE as a sole intermediate was detected. It indicates that a small fraction of ethanol was dissociated upon dark adsorption.

As shown in Fig. 7b, the bare TiO_2 efficiently decomposed ethanol into CO_2 and H_2O under UV light irradiation without producing any other by-products. In addition, the formation of acetaldehyde and acetic acid as by-products could be detected only in the initial stage of the photocatalytic reaction. These results have clearly demonstrated that when ethanol in air is treated by an air purification system with undetectable low content of terminal TiOH on the surface of non-defective and sufficiently reactive photocatalyts like the bare TiO_2 presented in this work, ethanol can be completely oxidized into harmless CO_2 and H_2O without any expanded off-odor problems. In contrast, in the photocatalytic oxidation over the F-TiO_2 and P25, the constant formation of ACE as a minor by-product was observed through the whole oxidation process, suggesting that ACE molecules forms at the same rate as they are oxidized. The carbon mass balance under the steady state calculated from acetaldehyde and CO_2 concentrations was closed within 10%. This testifies to the absence of important gaseous intermediates besides acetaldehyde. In addition, our results show a notably longer life time of the bare TiO_2 (more than one week), which further supports the carbon mass balance above.

By comparing with P25 TiO_2, the photocatalytic activity of both the bare TiO_2 and F-TiO_2 can be elevated simply by eliminating the terminal hydroxyl groups present on the TiO_2 surface. It has been reported that the terminal hydroxyl groups are basic in character, while the bridging hydroxyl groups possess acidic properties. The acid sites may be capable of increasing the adsorption of acetaldehyde/ethanol on the surface of TiO_2. These molecules interacting with the bridging hydroxyl groups can efficiently spill over, and form surface-bonded acetate/ethoxide intermediates. They can capture the photoinduced electrons more effectively, thus leading to an increase in the quantum yield. This is in good agreement with the observation by the groups of Anpo [24] and Zhao [25] that the presence of acid sites is beneficial for the photocatalytic reactivity. Instead of necessitating additional acid treatment of the surface as reported by them, the present work has found that the photocatalytic activity can be elevated simply by eliminating the terminal hydroxyl groups present on the TiO_2 surface.

The different photocatalytic behavior between the bare TiO_2 and F-TiO_2 could be associated with the different surface sites on TiO_2. Based on the ^{13}C solid-state NMR results from Raftery [26] and Deng [27], two types of adsorbed ethanol are also proposed

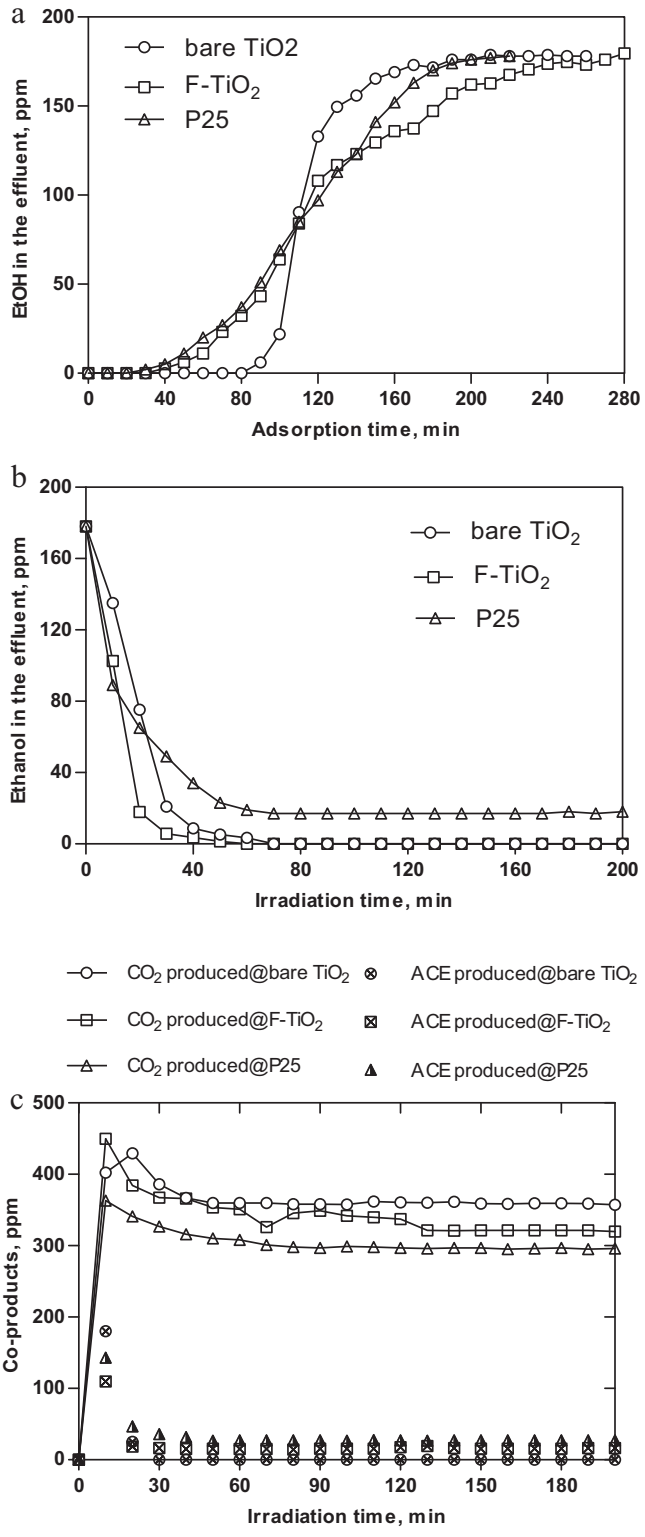

Fig. 7. Dark adsorption profile (a), photodegradation profiles (b), and the corresponding CO_2 and ACE produced (c) from photocatalytic oxidation of ethanol on bare TiO_2 (○), F-TiO_2 (□), and P25 (▲). Initial ethanol concentration = 178 ± 10 ppm.

to be formed on the bare TiO_2: a hydrogen bonded ethanol and a titanium-bonded ethoxide. Similar to the Deng's previous work on SO_4^{2-}/TiO_2, a new surface F-bound ethoxy (F-OCH_2CH_3) species may be presumably formed on the F-TiO_2 in addition to the above two groups. The constant formation of ACE from ethanol photocatalytic oxidation on F-TiO_2 is probably due to the presence of less reactive F-bound ethoxy species, which have long distance with the TiO_2 surface and may block the transfer of photogenerated holes. Therefore, to design a highly active photocatalysts is not utterly necessary to introduce foreign atoms, which may act as trap sites for the photo-excited charge carriers. As a good example, our present bare TiO_2 provides better photocatalytic performance than the F-modified TiO_2, which renders the wide application of the safe, abundant and inexpensive bare TiO_2.

4. Conclusions

This work confirmed the absence of surface terminal hydroxyl groups plays a key role in the photocatalytic oxidation of volatile organic compounds. Using a simple sonicated-assisted sol–gel method we can eliminate the surface terminal hydroxyl groups and achieve control over the distribution of hydroxyl groups present on the surfaces of the bare TiO_2 and F-TiO_2, as shown by high-field ^1H MAS NMR spectroscopy. Both of the bare TiO_2 and F-TiO_2 nanoparticles possess identical structural properties and exhibited high rate of photocatalytic oxidation (100%) of gaseous acetaldehyde and ethanol, respectively. It was also found that the F-TiO_2 degraded ethanol into dominating CO_2 along with minor acetaldehyde as a by-product. These results have clearly demonstrated that when ethanol in air is treated by an air purification system with non-defective and sufficiently reactive photocatalysts like the bare TiO_2 presented in this work, ethanol can be completely oxidized into harmless CO_2 and H_2O without any expanded off-odor problems. This work shows the feasibility to synthesize inexpensive and highly active TiO_2 through site engineering.

Acknowledgments

Financial support by the Australian Research Council through the ARC International Linkage Award with Boeing Company and ARC Discovery Early Career Researcher Award are gratefully acknowledged. We are indebted to UNSW Mark Wainwright Analytical Centre for the use of their instruments and the assistance from their staff.

Appendix A. Supplementary data

Supplementary data associated with this article can be found, in the online version, at http://dx.doi.org/10.1016/j.apcatb.2013.02.026

References

[1] K. Demeestere, J. Dewulf, H. Van Langenhove, Critical Reviews in Environmental Science and Technology 37 (2007) 489–538.
[2] M.R. Hoffmann, S.T. Martin, W. Choi, D.W. Bahnemann, Chemical Reviews 95 (1995) 69–96.
[3] A. Fujishima, K. Honda, Nature 238 (1972) 37–38.
[4] X. Chen, S.S. Mao, Chemical Reviews 107 (2007) 2891–2959.
[5] Y. Jiang, J. Scott, R. Amal, Applied Catalysis B: Environmental 126 (2012) 290–297.
[6] Y. Bessekhouad, D. Robert, J.V. Weber, Journal of Photochemistry and Photobiology A: Chemistry 157 (2003) 47–53.
[7] G. Oskam, A. Nellore, R.L. Penn, P.C. Searson, The Journal of Physical Chemistry B 107 (2003) 1734–1738.
[8] S.L. Lee, J. Scott, K. Chiang, R. Amal, Journal of Nanoparticle Research 11 (2009) 209–219.
[9] P.D. Cozzoli, A. Kornowski, H. Weller, Journal of the American Chemical Society 125 (2003) 14539–14548.
[10] W. Huang, X. Tang, Y. Wang, Y. Koltypin, A. Gedanken, Chemical Communications (2000) 1415–1416.
[11] J.C. Yu, J. Yu, W. Ho, L. Zhang, Chemical Communications (2001) 1942–1943.
[12] J.C. Yu, J. Yu, L. Zhang, W. Ho, Journal of Photochemistry and Photobiology A: Chemistry 148 (2002) 263–271.
[13] M. Crocker, R.H.M. Herold, A.E. Wilson, M. Mackay, C.A. Emeis, A.M. Hoogendoorn, Journal of the Chemical Society–Faraday Transactions 92 (1996) 2791–2798.

[14] Y. Jiang, J. Huang, W. Dai, M. Hunger, Solid State Nuclear Magnetic Resonance 39 (2011) 116–141.
[15] J. Zhang, Q. Xu, Z. Feng, M. Li, C. Li, Angewandte Chemie International Edition 47 (2008) 1766–1769.
[16] Y.K. Kho, A. Iwase, W.Y. Teoh, L. Maedler, A. Kudo, R. Amal, Journal of Physical Chemistry C 114 (2010) 2821–2829.
[17] T.A. Kandiel, L. Robben, A. Alkaim, D. Bahnemann, Photochemical and Photobiological Sciences (2013), http://dx.doi.org/10.1039/C2PP25217A.
[18] H. Zhang, J.F. Banfield, The Journal of Physical Chemistry B 104 (2000) 3481–3487.
[19] H. Zhang, J.F. Banfield, The Journal of Physical Chemistry C 111 (2007) 6621–6629.
[20] J. Zhang, M.J. Li, Z.C. Feng, J. Chen, C. Li, Journal of Physical Chemistry B 110 (2006) 927–935.
[21] J. Tang, H. Quan, J. Ye, Chemistry of Materials 19 (2006) 116–122.
[22] E. McCafferty, J.P. Wightman, Surface and Interface Analysis 26 (1998) 549–564.
[23] H. Kim, W. Choi, Applied Catalysis B: Environmental 69 (2007) 127–132.
[24] M. Takeuchi, T. Kimura, M. Hidaka, D. Rakhmawaty, M. Anpo, Journal of Catalysis 246 (2007) 235–240.
[25] Q. Wang, M. Zhang, C. Chen, W. Ma, J. Zhao, Angewandte Chemie International Edition 49 (2010) 7976–7979.
[26] S.J. Hwang, D. Raftery, Catalysis Today 49 (1999) 353–361.
[27] H. Zhang, H. Yu, A. Zheng, S. Li, W. Shen, F. Deng, Environmental Science and Technology 42 (2008) 5316–5321.